Journal of Groundwater Science and Engineering
ISSN 2305-7068
Indexed by ESCI CABI CSA
Scopus GeoRef AJ CNKI

**Web-based tool for analyzing the seawater-freshwater interface using analytical solutions and SEAWAT code comparison**

Asaad M. Armanuos, Mohamed Selmy, Hewida Omara, Bakenaz A. Zeidan, Sobhy R. Emara

Citation:
Armanuos Asaad M., Selmy M, Omara H, *et al*. 2025. Web-based tool for analyzing the seawater-freshwater interface using analytical solutions and SEAWAT code comparison. Journal of Groundwater Science and Engineering, 13(3): 250-267.

View online: https://doi.org/10.26599/JGSE.2025.9280053

**Articles you may be interested in**

Using time series analysis to assess tidal effect on coastal groundwater level in Southern Laizhou Bay, China
Journal of Groundwater Science and Engineering. 2022, 10(3): 292-301 https://doi.org/10.19637/j.cnki.2305-7068.2022.03.007

Analytical solutions for constant-rate test in bounded confined aquifers with non-Darcian effect
Journal of Groundwater Science and Engineering. 2022, 10(4): 311-321 https://doi.org/10.19637/j.cnki.2305-7068.2022.04.001

Development, hotspots and trend directions of groundwater numerical simulation: A bibliometric and visualization analysis
Journal of Groundwater Science and Engineering. 2024, 12(4): 411-427 https://doi.org/10.26599/JGSE.2024.9280031

State of seawater intrusion and its adaptive management countermeasures in Longkou City of China
Journal of Groundwater Science and Engineering. 2020, 8(1): 30-42 https://doi.org/10.19637/j.cnki.2305-7068.2020.01.004

Numerical simulation and environmental impact prediction of karst groundwater in Sangu Spring Basin, China
Journal of Groundwater Science and Engineering. 2020, 8(3): 210-222 https://doi.org/10.19637/j.cnki.2305-7068.2020.03.002

Numerical simulation of operation performance on production and injection of a double well geothermal system in Kailu Basin, Inner Mongolia
Journal of Groundwater Science and Engineering. 2022, 10(2): 196-208 https://doi.org/10.19637/j.cnki.2305-7068.2022.02.008

*Journal of Groundwater Science and Engineering* 13(2025) 250–267

Journal homepage: http://gwse.iheg.org.cn

Research Article

# Web-based tool for analyzing the seawater-freshwater interface using analytical solutions and SEAWAT code comparison

Asaad M. Armanuos[1], Mohamed Selmy[1], Hewida Omara[1], Bakenaz A. Zeidan[1], Sobhy R. Emara[1*]

[1] *Irrigation and Hydraulics Engineering Department, Faculty of Engineering, Tanta University, Tanta, Egypt.*

**Abstract:** Saltwater Intrusion (SI) poses a significant environmental threat to freshwater resources in coastal aquifers globally. The primary objective of this research is to illustrate the variations in the saltwater-freshwater interface using several established analytical solutions, integrated within a user-friendly web-based tool. Three case studies, including a hypothetical unconfined coastal aquifer, an experimental coastal aquifer, and a real-world coastal aquifer in Gaza, were applied to examine the interface dynamics using the developed tool, built with JavaScript. To simulate variable-density flow within the Gaza coastal aquifer, the public domain code SEAWAT was employed. The resulting lengths of seawater intrusion, as simulated by SEAWAT and the observed toe length, were compared with those obtained from the web-based analytical solutions under both constant head and constant flux boundary conditions. This comparison demonstrated a strong correlation between the experimental results, SEAWAT model outputs, and analytical solutions. This research provides valuable insights into SI in coastal aquifers, with a specific focus on the impact of Sea Level Rise (SLR) on the shifting position of the seawater intrusion toe. The outcomes are presented through an accessible web-based interface, thereby promoting broader dissemination and practical application of the research outcomes.

**Keywords:** Saltwater Intrusion; Numerical Simulation; Coastal Aquifers; Sea Level Rise; SEAWAT

Received: 12 Jul 2024/ Accepted: 30 Mar 2025/ Published: 27 Jun 2025

## Introduction

Saltwater Intrusion (SI), the infiltration of saline seawater into coastal aquifer systems, represents a significant threat to coastal habitats worldwide, particularly in regions where groundwater serves as the primary source of freshwater. Under normal conditions, groundwater flows towards the sea, effectively preventing the encroachment of salinity into aquifers. However, excessive groundwater extraction can lead to a decline in groundwater levels, thereby reducing freshwater discharge and intensifying the effects of SI (Werner et al. 2013; Emara et al. 2024a). Consequently, effective management and a thorough understanding of coastal aquifers are crucial for ensuring global water security. These challenges highlight the vital importance of comprehending and managing these systems to safeguard water resources worldwide.

Climate change exerts a considerable influence on saltwater intrusion through various mechanisms. Directly, it contributes to Sea Level Rise (SLR). Indirectly, it can lead to reduced rainfall in certain areas, resulting in decreased natural recharge and drought conditions. These impacts can cause the saltwater wedge to extend further inland, a problem exacerbated by excessive groundwater withdrawal (Ataie-Ashtiani et al. 2013; Abdoulhalik and Ahmed, 2017; Emara et al. 2023a). These vulnerabilities highlight the urgent need to address SI dynamics within the context of climate variability.

*Corresponding author: Sobhy R. Emara, *E-mail address*: sobhy_emara39@f-eng.tanta.edu.eg

DOI: 10.26599/JGSE.2025.9280053

Armanuos Asaad M., Selmy M, Omara H, et al. 2025. Web-based tool for analyzing the seawater-freshwater interface using analytical solutions and SEAWAT code comparison. Journal of Groundwater Science and Engineering, 13(3): 250-267.

2305-7068/© 2025 Journal of Groundwater Science and Engineering Editorial Office This is an open access article under the CC BY-NC-ND license (http://creativecommons.org/licenses/by-nc-nd/4.0)

Globally, freshwater resources are increasingly threatened by saltwater intrusion driven by SLR (Dang et al. 2020). Both analytical solutions (Ataie-Ashtiani et al. 2013; Lu et al. 2016) and numerical groundwater modeling (Sherif et al. 2014; Abd-Elaty and Zelenakova, 2022; Emara et al. 2024b) are effective methods for simulating the dynamic process of saltwater intrusion. Analytical techniques provide straightforward approaches to estimate the freshwater-saltwater interface, while numerical models offer intricate simulations for complex scenarios, although they remain dependent on computational resources and calibration data.

Koussis et al. (2012) established steady-state analytical techniques to determine the position of the seawater-freshwater interface wedge toe between the freshwater and saltwater zones. Their approach assumed a sharp interface SI within a sloping coastal unconfined aquifer under a constant groundwater recharge rate. Lu et al. (2015) developed analytical methods that incorporated an inland general-head boundary condition for SI in both confined and unconfined coastal aquifers. They applied these solutions to predict the movement of the interface toe in response to a 1-meter SLR. Furthermore, Lu et al. (2016), also assuming a sharp-interface SI, developed steady-state analytical approaches for SI in sloping confined and unconfined coastal aquifers. Anderson (2021) presented an analytical approach for the groundwater flow interface in an anisotropic unconfined coastal aquifer of finite depth. Based on sharp-interface assumptions, Luo et al. (2022) developed analytical approaches for steady-state SI in unconfined coastal aquifers, accounting for unsaturated flow within the analytical model of the discharge formula. While these techniques offer valuable insights, their reliance on sharp-interface assumptions may limit their ability to fully capture the complexities of variable-density flow.

Emara et al. (2023) integrated numerical and experimental methods to investigate SI in two homogeneous aquifers under conditions of SLR and varying freshwater inflow. Their research compared transient-state saltwater concentrations and groundwater heads from numerical models with experimental data for both advancing and receding saltwater fronts. Ten steady-state SI wedge and toe length experimental tests were evaluated against seven analytical solutions. The study highlighted the significant influence of inland water head and the SLR on SI dynamics. Ataie-Ashtiani et al. (2013) employed a direct analytical method to assess the impact of land-surface inundation on SLR-induced SI dynamics in simplified settings. The results indicate that significant submergence of the ground surface significantly expands SI boundaries, potentially resulting in inland penetration several times greater than shoreline pressure alterations in open coastal aquifers under realistic conditions.

An analytical formula for calculating the precise location of the saltwater-freshwater interface was independently derived by Badon Ghyben (1888) and Herzberg (1901). Their formula establishes a relationship between the elevation of the water table in an unconfined aquifer and the depth to the interface. To determine the location of the sharp seawater-freshwater interface in a coastal groundwater aquifer, Glover (1959) subsequently developed an equation that incorporates the seaward flow of freshwater. Building upon Glover's work, Rumer Jr and Harleman (1963) examined the parabolic shape of the interface, a characteristic further demonstrated by Verruijt (1968). Using laboratory-scale experiments, Goswami and Clement (2007) developed a benchmark model to simulate seawater intrusion and investigated the dynamics of the saltwater wedge under both steady-state and transient conditions.

Chang et al. (2011) investigated whether variations in freshwater discharge and sea level rise could impact both unconfined and confined groundwater aquifers. The effect of spatial variations in tidal dynamics and freshwater influx on SI in coastal aquifers was elucidated by Kuan et al. (2012).

Researchers have proposed several engineering techniques to mitigate saltwater intrusion and preserve groundwater quality in coastal regions. These include employing negative hydraulic barriers, such as inland seawater abstraction (Javadi et al. 2015; Mehdizadeh et al. 2019); optimizing abstraction well configurations (Fan et al. 2020; Ranjbar et al. 2020); implementing artificial recharge through injection and infiltration (Motallebian et al. 2019; Armanuos et al. 2020a); and constructing underground dams and cutoff walls (Kaleris and Ziogas, 2013; Armanuos et al. 2020b; Emara et al. 2023b).

This study aims to investigate the variations in the seawater–freshwater interface under different conditions, using a range of established analytical solutions presented through an interactive web-based tool. Developed in JavaScript, the tool was tested using three case studies: A hypothetical unconfined coastal aquifer (Sun et al. 2021), a laboratory-scale experimental aquifer, and a real-world coastal aquifer in Gaza. These case studies

serve to evaluate the tool's performance and versatility in visualizing and analyzing interface dynamics. For the Gaza aquifer specifically, the SEAWAT code was used to simulate variable-density groundwater flow, providing a more detailed and realistic understanding of the interface behavior in that particular region.

## 1 Methodology

In this research, SEAWAT was used to develop numerical models for groundwater flow that simulate the transport of salt within coastal aquifers. The saltwater intrusion wedge simulated by SEAWAT was validated against analytical approaches. Specifically, the analytical solutions and the resulting simulated intrusion lengths from Ataie-Ashtiani et al. (2013) were compared under both constant head and constant flux boundary conditions. The research encompasses two case studies: A hypothetical unconfined coastal aquifer (Sun et al. 2021) and the Gaza coastal aquifer in Palestine. The steady-state seawater wedges resulting from these simulations were contrasted with the analytical solutions established by Ghyben (1888), Glover (1959), Rumer Jr and Harleman (1963), and Verruijt (1968). The study particularly focused on the Gaza coastal aquifer, where the simulated intrusion lengths of the SI wedge toe, obtained using the SEAWAT code, were compared with the values calculated by Ataie-Ashtiani et al. (2013). This comparison was facilitated through a web-based interface tool, which also enabled the examination of various sea level rise scenarios.

### 1.1 Numerical Model (SEAWAT)

SEAWAT has been widely utilized for simulating variable density groundwater (GW) flow (Guo and Langevin, 2002). To evaluate the impact of SLR on coastal GW aquifers, a numerical simulation of solute transport was developed in this research using SEAWAT.

The flow and transport equations employed in SEAWAT are presented in Equations (1) and (2), respectively.

$$\frac{\partial}{\partial \mathrm{X}}\left(\rho \mathrm{k}_{\mathrm{fX}}\left[\frac{\partial \mathrm{h}_{\mathrm{f}}}{\partial \mathrm{X}}+\frac{\rho-\rho_{\mathrm{f}}}{\rho_{\mathrm{f}}} \frac{\partial \mathrm{Z}}{\partial \mathrm{X}}\right]\right)+ \frac{\partial}{\partial \mathrm{Y}}\left(\rho \mathrm{k}_{\mathrm{fY}}\left[\frac{\partial \mathrm{h}_{\mathrm{f}}}{\partial \mathrm{Y}}+\frac{\rho-\rho_{\mathrm{f}}}{\rho_{\mathrm{f}}} \frac{\partial \mathrm{Z}}{\partial \mathrm{Y}}\right]\right)+ \frac{\partial}{\partial \mathrm{Z}}\left(\rho \mathrm{k}_{\mathrm{fZ}}\left[\frac{\partial \mathrm{h}_{\mathrm{f}}}{\partial \mathrm{Z}}+\frac{\rho-\rho_{\mathrm{f}}}{\rho_{\mathrm{f}}} \frac{\partial \mathrm{Z}}{\partial \mathrm{Z}}\right]\right)= \rho \mathrm{S}_{\mathrm{f}} \frac{\partial \mathrm{h}_{\mathrm{f}}}{\partial \mathrm{t}}+\theta \frac{\partial \rho}{\partial \mathrm{C}} \frac{\partial \mathrm{C}}{\partial \mathrm{t}}-\rho_{\mathrm{s}} \mathrm{q}_{\mathrm{s}} \quad (1)$$

Where: $X$, $Y$, and $Z$ are the direction of the groundwater flow; $t$ is time; $k_{fX}$, $k_{fY}$, and $k_{fZ}$ are the hydraulic conductivities of the porous media in $X$, $Y$, and $Z$ direction; $\theta$ is the effective porosity; $S_f$ is the specific storage; $\rho_f$ is the density of fresh groundwater; $\rho$ is the density of the groundwater at a point in the coastal aquifer; $\rho_S$ is the density of the dissolved material, and $q_S$ is the volumetric flow rate, correspondingly.

$$\frac{\partial\left(\theta C^{k}\right)}{\partial \mathrm{t}}=\nabla\left(\theta \mathrm{D}_{\mathrm{ij}} \nabla C^{k}\right)-\nabla\left(\theta V_{i} C^{k}\right)+\mathrm{q}_{\mathrm{s}} C_{k}^{\mathrm{S}}+\sum R_{n} \quad (2)$$

Where: $C^k$ represents the concentration of the solute substance; $\sum R_n$ defines the reaction process term of the chemical substance in the coastal aquifer system; $D$ is the coefficient tensor of the hydrodynamic dispersion coefficient; $V_i$ represents the average linear fluid velocity; $C_k^S$ represents the source or sink concentration of species $k$.

### 1.2 Analytical equations

The resulting steady state seawater wedges were compared against the analytical solutions provided by Ghyben (1888), Glover (1959), Rumer Jr and Harleman (1963), and Verruijt (1968).

Independently, Badon Ghyben (1888) and Herzberg (1901) developed an analytical equation for determining the position of the sharp saltwater-freshwater interface. Their equation correlates the depth to the interface with the elevation of the water table in an unconfined aquifer. Subsequently, Glover (1959) formulated an expression to describe the sharp seawater- freshwater interface in a coastal GW aquifer, considering the seaward flow of freshwater. This expression can be used to determine the interface location. Building on Glover's work, Rumer Jr and Harleman (1963) analyzed the parabolic shape of the interface. Verruijt (1968) further established that the seawater-freshwater interface follows a parabolic profile.

Table 1 presents the analytical equations for the seawater-freshwater interface according to the solutions by Ghyben (1888) and Herzberg (1901), Rumer Jr and Harleman (1963), and Verruijt (1968). Table 2 presents the analytical equations of Ataie-Ashtiani et al. (2013) for assessing the influence of SLR on the toe of seawater (SW) - freshwater (FW) interface, specifically for constant flux and constant head boundary conditions.

## 2 Case studies

Three case studies were implemented to demon-

**Table 1** Analytical Equations implemented in the Seawater (SW)-Freshwater (FW) Interface Web-Based Model

| Seawater (SW)-Freshwater Interface Web-Based Model | Analytical Equations |
|---|---|
| Badon Ghyben (1888) & Herzberg (1901) | $z = \frac{\rho_f}{\rho_s - \rho_f} h_f$ |
| Glover (1959) | $z^2 = \frac{2\rho_f q x}{\Delta\rho K} + \left(\frac{\rho_f q}{\Delta\rho K}\right)^2$ |
| Rumer Jr and Harleman (1963) | $z^2 = \frac{2\rho_f q x}{\Delta\rho K} + 0.55\left(\frac{\rho_f q}{\Delta\rho K}\right)^2$ |
| Verruijt (1968) | $Z = -\left(\left(\frac{q}{\beta K}\right)^2 \cdot \left(\frac{1-\beta}{1+\beta}\right) + 2\left(\frac{q}{\beta K}\right) \cdot \left(\frac{x}{1+\beta}\right)\right)^{1/2}$ |

Where: $\rho_s$ (M L$^{-3}$) represents the seawater density, $\rho_f$ (M L$^{-3}$) represents the fresh groundwater density, $z$ (L) represents the depth to a point on the seawater-freshwater interface under the mean sea level, and $h_f$ (L) represents the elevation of the water table in the aquifer measured above the mean sea level at the same point, $q$ (L$^2$ T$^{-1}$) represents the rate of the fresh groundwater discharge, $K$ (LT$^{-1}$) denotes the hydraulic conductivity of the aquifer medium, $\Delta\rho = \rho_s - \rho_f$, x (L) represents the horizontal distance calculated from the shore line and $\beta = (\rho_s - \rho_f)/\rho_f$.

**Table 2** Analytical equations for the influence of Sea Level Rise (SLR) on Toe of Seawater (SW)-Freshwater (FW) Interface (Ataie-Ashtiani et al. 2013)

| | | |
|---|---|---|
| **Constant Flux Boundary** | **Steady-state SI toe** | $X_T = \left(\frac{q}{W} + L\right) - \sqrt{\left(\frac{q}{W} + L\right)^2 - \frac{K\delta(1+\delta)z_o^2}{W}}$ |
| | **Impact of SLR on the toe of SW-FW interface** | $X_T^{'} = \left(\frac{q}{W} + L - \frac{\Delta z}{s}\right) - \sqrt{\left(\frac{q}{W} + L - \frac{\Delta z}{s}\right)^2 - \frac{K\delta(1+\delta)(z_o+\Delta z)^2}{W}} + \frac{\Delta z}{s}$ |
| Constant Head Boundary | Steady state SI toe | $q = \frac{K((h_b+z_o)^2 - (1+\delta)z_o^2)}{2L} - \frac{WL}{2}$ |
| | | $X_T = \left(\frac{q}{W} + L\right) - \sqrt{\left(\frac{q}{W} + L\right)^2 - \frac{K\delta(1+\delta)z_o^2}{W}}$ |
| | Impact of SLR on toe of SW-FW interface | $q = \frac{K\left((h_b+z_o)^2 - (1+\delta)(z+\Delta z)^2\right)}{2\left(L - \frac{\Delta z}{s}\right)} - \frac{W\left(L - \frac{\Delta z}{s}\right)}{2}$ |
| | | $X_T^{'} = \left(\frac{q}{W} + L - \frac{\Delta z}{s}\right) - \sqrt{\left(\frac{q}{W} + L - \frac{\Delta z}{s}\right)^2 - \frac{K\delta(1+\delta)(z_o+\Delta z)^2}{W}} + \frac{\Delta z}{s}$ |

Where: $X_T$ (L) represents the position of the toe calculated from the sea boundary, $z$ (L) represents the mean sea level rise, $X_T^{'}$ (L) represents the new position of the seawater-freshwater wedge toe calculated from the costal line boundary subsequently the Sea Level Rise (SLR), $K$ (L T$^{-1}$) represents the hydraulic conductivity of the groundwater aquifer system, $L$ (L) represents the coastal aquifer length, $q$ (L$^2$ T$^{-1}$) represents the fresh groundwater flow within the coastal aquifer boundary calculated per of the coastline aquifer unit width, $z_o$ (L) represents the coastal aquifer depth bottom calculated from the mean sea level, $W$ (L T$^{-1}$) represents the rate groundwater uniform recharge, and $\delta$ (−) represents the dimensionless value of the density term equal to $(\rho_s - \rho_f)/\rho_f$, where $\rho_f$ (M L$^{-3}$) is the density of the freshwater and $\rho_s$ (M L$^{-3}$) represents the density of the saltwater, $s$ represents the slope of the seaward boundary of the aquifer. The public value of 0.025 is adopted for δ.

strate the application of the web-based tool for analyzing the seawater-freshwater interface. These include a hypothetical unconfined coastal aquifer, an experimental case study, and an application to Gaza coastal aquifer was employed.

## 2.1 Hypothetical unconfined coastal aquifer

First, the seawater-freshwater interface of a hypothetical unconfined coastal aquifer (Table 3), as predicted by the analytical equations by Ghyben (1888), Glover (1959), Rumer Jr and Harleman (1963), and Verruijt (1968), was compared with the numerical solutions using the developed SW-FW web-based tool. Second, the position of the seawater-freshwater wedge toe in the Gaza coastal aquifer, as simulated by the SEAWAT code, was compared with the analytical solution of Ataie-Ashtiani et al. (2013) using the same SW-FW interface web-based tool.

## 2.2 Experimental case study

A sandbox tank with dimensions of 74.4 cm (length), 35 cm (height), and 10 cm (breadth) was used to conduct the seawater intrusion experiment. The unconfined coastal aquifer in the center of the sandbox model was modeled using silica sand number 4 as the porous medium. Each end of the sandbox model contained 5.0 cm deep layers of sand. The freshwater boundary had a concentra-

**Table 3** Numerical model parameters for the hypothetical unconfined coastal aquifer (from Sun et al. 2021)

| Parameter | Description | Value | Units |
|---|---|---|---|
| L | Aquifer length | 500 | m |
| H | Aquifer depth | 50 | m |
| n | Porosity | 0.30 | -- |
| K | The hydraulic conductivity | 30 | m/d |
| $\alpha_l$ | The longitudinal dispersivity | 1.0 | m |
| $\alpha_t$ | The transverse dispersivity | 0.1 | m |
| $\rho_f$ | The density of the fresh groundwater | 1,000 | Kg/m$^3$ |
| $\rho_s$ | The density of saline water | 1,025 | Kg/m$^3$ |
| **Boundary condition** | | | |
| $h_s$ | Seawater hydraulic head | 50 | m |
| $q_f$ | Freshwater inflow | 0.2 | m/d |
| $C_s$ | Saltwater concentration | 35,000 | mg/L |
| $C_f$ | The concentration of the freshwater | 1,000 | mg/L |

tion of 1,000 mg/L, while the seawater boundary had a concentration of 35,000 mg/L. The measured density of the freshwater solution was 1,000 kg/m$^3$, and that of the saltwater solution was 1,025 kg/m$^3$. Initially, the freshwater and saltwater heads were set at the same height (30.50 cm) for each experiment, allowing seawater to intrude inland into the aquifer. After 55 minutes, the length of the saltwater intrusion wedge had extended to 64.0 cm. Subsequently, the freshwater head in the freshwater tank was raised from 30.50 cm to 31.40 cm, while the saltwater head remained constant at 30.50 cm throughout the remainder of the experiment. This increase in freshwater head created a head difference of 0.90 cm, causing the freshwater flow to push the saltwater wedge back towards the saltwater reservoir.

The outflow from drainage pipes was used to estimate the freshwater flow rate and hydraulic conductivity from the freshwater side to the saltwater side. Based on the experiments, the estimated fluctuations in head were ±1.0 mm. The hydraulic gradient established by the head difference between the two reservoirs drove a flow from the freshwater reservoir to the saltwater reservoir. Darcy's law was applied to the hydraulic gradient and the measured freshwater flow from the drainage pipes to calculate the hydraulic conductivity (K) of the porous medium in the sand tank. The average porosity and hydraulic conductivity were determined to be 0.43 cm/sec and 0.60 cm/sec, respectively. Fig. 1 illustrates the saltwater intrusion wedge at time intervals of 15, 30, 45, 60, 75, and 95 minutes after the head difference was increased to 0.90 cm. Following the head increase, the saltwater wedge progressively receded, reaching a steady-state condition with a length of 48.0 cm (measured from the saltwater reservoir) after 95 minutes, at which point no further discernible change in the toe position was observed.

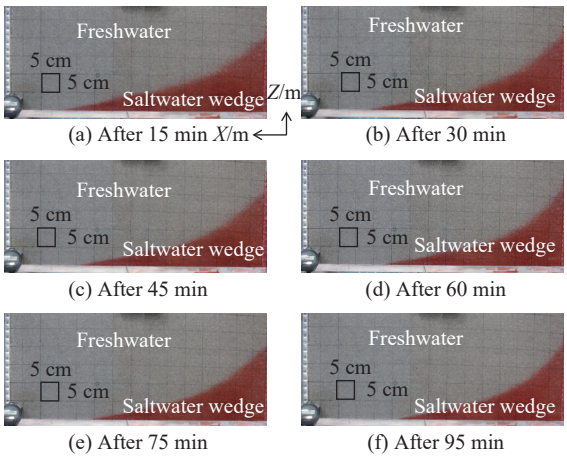


**Fig. 1** Saltwater intrusion wedge evolution over time (15, 30, 45, 60, 75, and 95 minutes) after increasing the freshwater head to 31.40 cm

## 2.3 Real case study (Gaza Coastal aquifer)

The Gaza Strip (GS) is a narrow coastal region situated along the plain of the Mediterranean Sea, between Egypt and Palestine. Geographically, it is located between longitudes 34° 13′ and 34° 33′ east and latitudes 31° 13′ and 31° 36′ north, covering an area of 365 square kilometers with a 45-kilometer coastline. Its width ranges from 6 kilometers to 12 kilometers from north to south, with an average width of 9 kilometers (Heen and Muhsen, 2016), as depicted in Fig.

2. The GS is one of the most densely populated regions globally (Abd-Elaty and Zelenakova, 2022). This high population density leads to an increased demand for groundwater resources, resulting in greater abstraction from the aquifer and consequently exacerbating seawater intrusion.

Abualtayef et al. (2017) evaluated the hydraulic properties of the quaternary aquifer through in-site investigations and pumping tests, thereby characterizing its hydraulic behavior. The estimated transmissivity values ranged from 700 $m^2$/day to 5,000 $m^2$/d, while the hydraulic conductivity varied from 20 m/d to 80 m/d. For the unconfined aquifer, the specific yield was determined to be in the range of 0.15 to 0.30. In contrast, the confined units exhibited a specific storage value of $10^{-4}$ $m^{-1}$. Qahman (2004) estimated the longitudinal dispersivity ($\alpha_L$) and transverse dispersivity ($\alpha_T$) to be 50 m and 0.10 m, respectively, and the effective porosity to be 0.35. Table 4 presents the boundary conditions and hydraulic parameters used for the Gaza coastal aquifer model.

## 3 Results and discussion

### 3.1 Results of seawater-freshwater interface web-based code for hypothetical coastal aquifer

Fig. 3 illustrates the input parameters for the seawater-freshwater interface calculations using

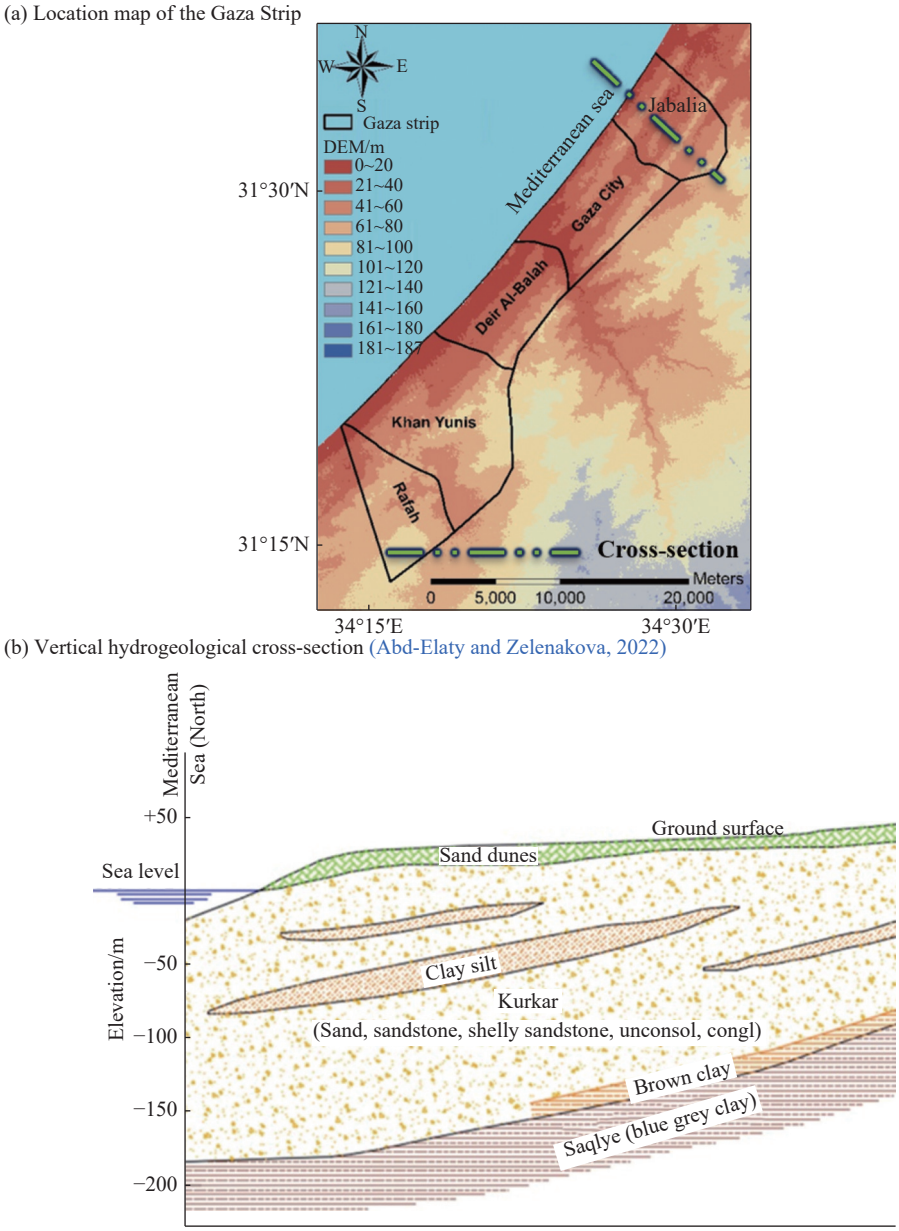


**Fig. 2** Gaza shallow coastal aquifer

**Table 4** Boundary conditions and hydraulic parameters used for Gaza aquifer model

| **Boundary condition** | **Value** | | **Unit** |
|---|---|---|---|
| The flux of the lateral freshwater | 10 | | $m^3/d/m$ |
| Well abstraction rates | 20.75 | | $m^3/d/m$ |
| Vertical recharge rate and the return flow | 416.5 | | mm/year |
| The head of the saltwater $h_s$ | Zero | | m |
| The concentration of the seaside boundary | 35000 | | mg/L |
| The concentration of the land side boundary | 1000 | | mg/L |
| **Hydraulic parameters** | **Confined aquifer** | **Unconfined aquifer** | **Unit** |
| The hydraulic conductivity in the horizontal ($K_h$) | 0.2 | 34 | m/d |
| The hydraulic conductivity in the vertical direction ($K_v$) | 0.02 | 3.4 | m/d |
| The value of the Effective porosity ($n_e$) | 0.3 | 0.25 | - |
| Total Porosity ($n_t$) | 0.45 | 0.35 | - |
| The density of the fresh groundwater | 1000 | 1000 | $Kg/m^3$ |
| The density of the saline water | 1025 | 1025 | $Kg/m^3$ |
| Specific storage | 0.00001 | 0.0001 | - |
| Longitudinal dispersivity | 50 | 12 | - |
| Transverse dispersivity | 5 | 1.2 | - |
| Molecular diffusion coefficient (D) | 0.0001 | 0.0001 | $m^2/d$ |

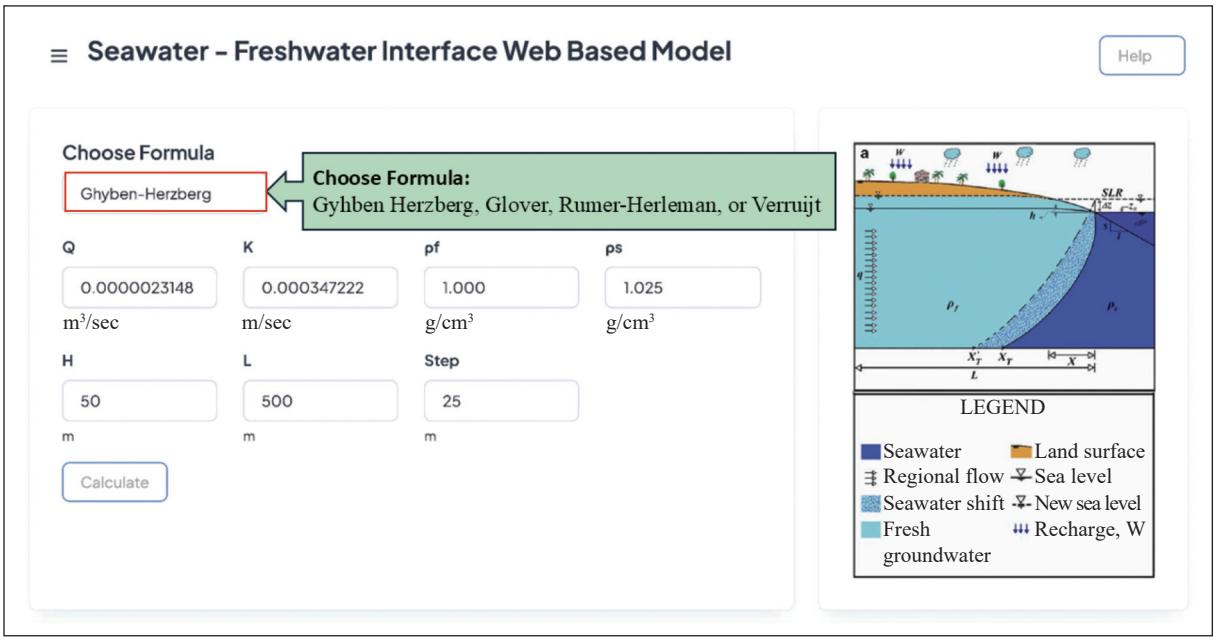


**Fig. 3** Input parameters for calculating the seawater-freshwater interface for the hypothetical coastal aquifer using the analytical solutions Gyhben Herzberg, Glover, Rumer-Herleman, and Verruijt

the following analytical solutions: Gyhben Herzberg, Glover, Rumer-Herleman, and Verruijt. These input parameters include the coastal aquifer length, the aquifer depth from the mean sea level to the bottom of the groundwater aquifer system, the density of freshwater, the density of saltwater, the freshwater flux boundary, and the hydraulic conductivity. For the hypothetical unconfined coastal aquifer, the assigned input parameters were: L = 500 m, H = 50 m, the density of the fresh groundwater = 1.0 $gm/cm^3$, the density of the saline water = 1.025 $gm/cm^3$, K = 0.000347 cm/sec, and Q = $2.31x10^{-6}$ $m^3$/sec. The step value, representing the interval along the x-axis at which the interface depth is calculated by the different solutions, was set to 25 m. The resulting seawater-freshwater interfaces for the Gyhben-Herzberg, Glover, Rumer-Herleman, and Verruijt analytical solutions are presented in Fig. 4. The intrusion length of the saline water is calculated from the

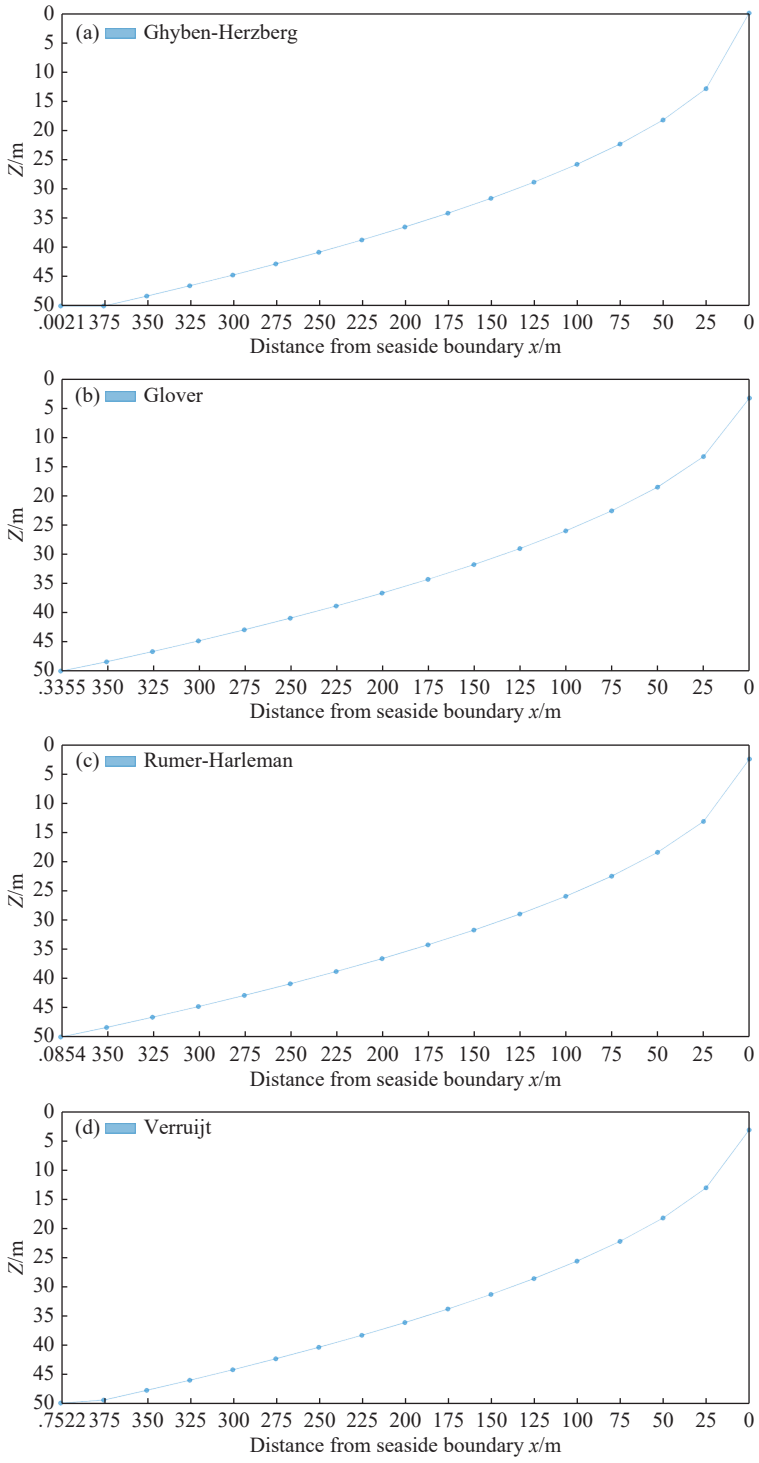


**Fig. 4** Seawater-freshwater interface for a hypothetical coastal aquifer based on the analytical solutions of: (a) Gyhben Herzberg, (b) Glover, (c) Rumer-Herleman, and (d) Verruijt

coastline boundary. The calculated lengths of the seawater wedge toe were 375.021 m, 350.335 m, 350.09 m, and 382.75 m for Gyhben-Herzberg, Glover, Rumer-Herleman, and Verruijt, respectively. The simulated toe length for the same hypothetical unconfined coastal aquifer by Sun et al. (2021) was 340 m. Fig. 5 presents a comparison between the simulated seawater-freshwater interface for the hypothetical unconfined coastal aquifer by (Sun et al. 2021) and the analytical solutions of Gyhben-Herzberg, Glover, Rumer-Herleman, and Verruijt, as generated through the web-based interface model. The comparison between the simulated and analytical results of the seawater-freshwater interface indicates a good agreement. Furthermore, the Glover and Rumer-Herleman

solutions appear to provide the most accurate estimations of the seawater intrusion wedge toe and its penetration length.

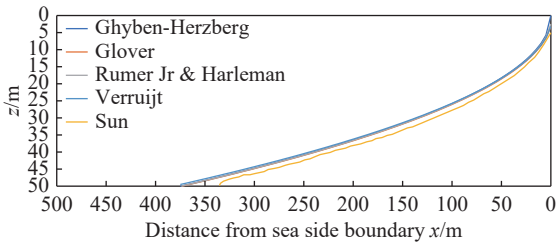


**Fig. 5** Comparison between the simulated SW-FW interface for the hypothetical unconfined coastal aquifer (from Sun et al. 2021) and the analytical solutions of Gyhben-Herzberg, Glover, Rumer-Herleman, and Verruijt through the web-based interface model

## 3.2 Results of seawater-freshwater interface web-based code for experimental coastal aquifer

Fig. 6 displays the input parameters for the seawater-freshwater interface for the experimental costal aquifer using the Gyhben Herzberg, Glover, Rumer-Herleman, and Verruijt solutions. The considered input factors include the aquifer's coastal length, its depth from the mean sea level to the bottom of the groundwater system, the freshwater and saltwater densities, the freshwater flux boundary, and the hydraulic conductivity value. The specific input parameters assigned to the experimental unconfined coastal aquifer were: the fresh groundwater density = 1.0 gm/cm$^3$, the salty water density = 1.025 gm/cm$^3$, K = 0.006 m/sec, Q = $0.114\times10^{-7}$ m$^3$/sec, L = 0.744 m, and H = 0.305 m. The step value, representing the distance along the x-axis at which the interface's depth is computed by the various solutions, was set to 0.005 m. Fig. 7 shows the seawater-freshwater interface for the experimental coastal aquifer as predicted by the Gyhben-Herzberg, Glover, Rumer-Herleman, and Verruijt analytical solutions. The intrusion length of the saline water is calculated from the coastline. The estimated seawater wedge toe lengths were 48.961 cm, 48.96 cm, 48.96 cm, and 50.184 cm for Gyhben Herzberg, Glover, Rumer-Herleman, and Verruijt, respectively. According to experimental observations by Armanuos (2017), the toe length was 48 cm. Fig. 8 presents a comparison between the analytical results from the web-based interface model for Gyhben-Herzberg, Glover, Rumer-Herleman, and Verruijt, and the simulated seawater-freshwater interface for the experimental unconfined coastal aquifer by Armanuos (2017). A good agreement was observed between the experimental and analytical results regarding the freshwater-saltwater interface. Furthermore, the Glover and Rumer-Herleman solutions appear to offer the most accurate estimations of both the seawater intrusion wedge toe and its penetration length.

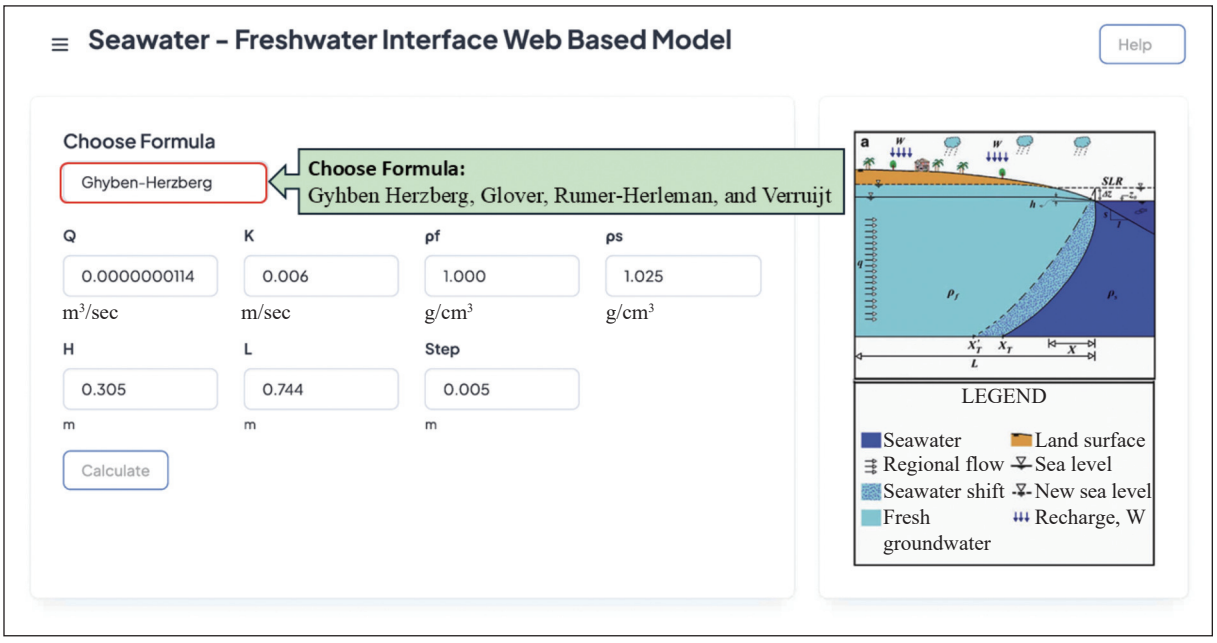


**Fig. 6** Input Parameters for calculating the seawater-freshwater interface using the analytical solutions of Gyhben-Herzberg, Glover, Rumer-Herleman, and Verruijt for the experimental coastal aquifer

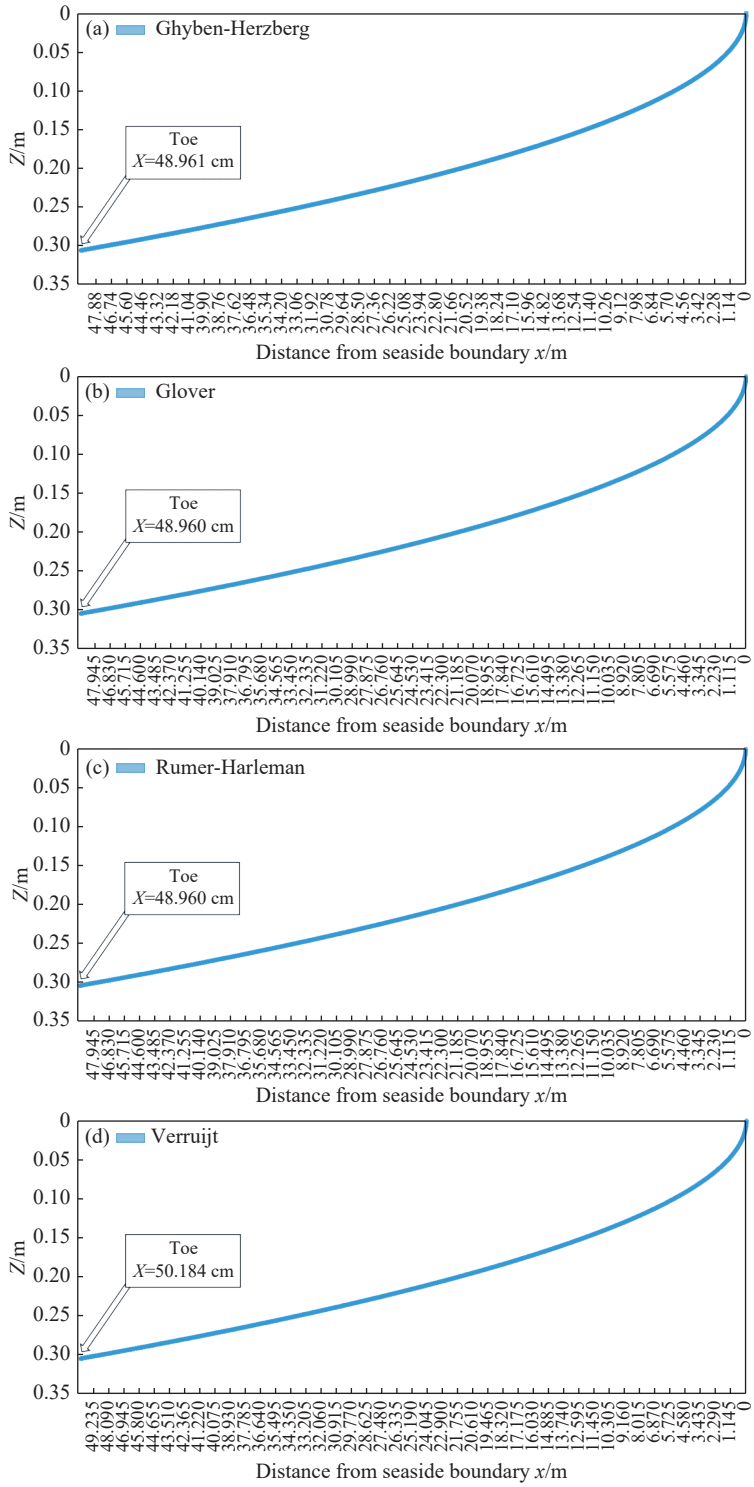


**Fig. 7** Seawater-freshwater interface for the experimental coastal aquifer based on the analytical solutions of: (a) Gyhben-Herzberg, (b) Glover, (c) Rumer-Herleman, and (d) Verruijt

### 3.3 Results of the influence of the rise in Sea Level on the saline water intrusion in Gaza groundwater coastal aquifer, Palestine

The groundwater head in the Gaza coastal aquifer ranges from 0.0 (sea level) to −4.6 m, as shown in Fig. 9. Fig. 10 illustrates the outcome of the calibration process, comparing the simulated and observed heads from 15 monitoring wells with the observed heads reported by Sirhan and Koch (2013) at the end of 2010. The residuals between the simulated and observed heads range from

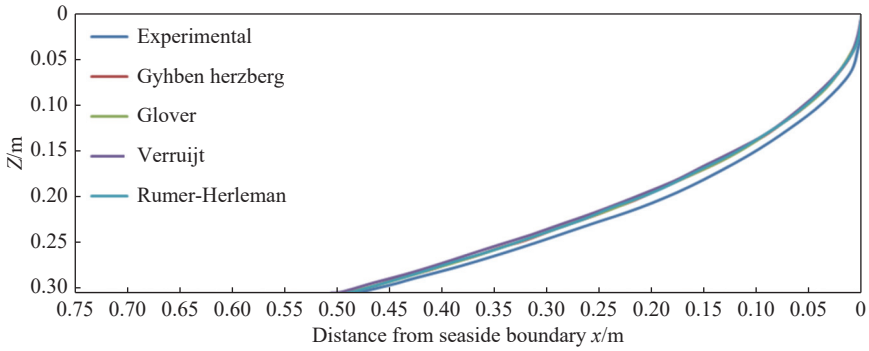


**Fig. 8** Comparison between the experimental SW- FW interface for the experimental unconfined coastal aquifer (from Armanuos, 2017) and the analytical solutions for Gyhben-Herzberg, Glover, Verruijt, and Rumer-Herleman through the web-based interface

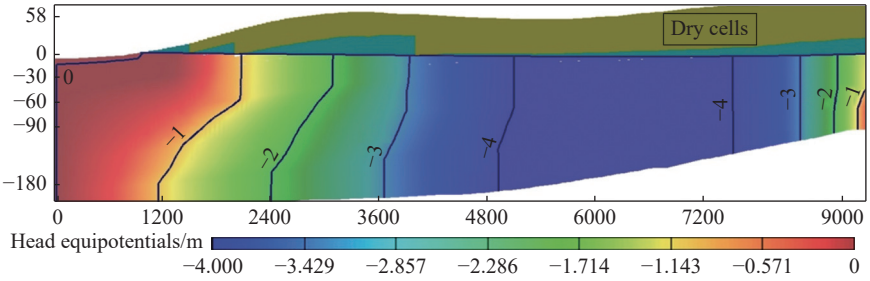


**Fig. 9** Groundwater head in the GCA

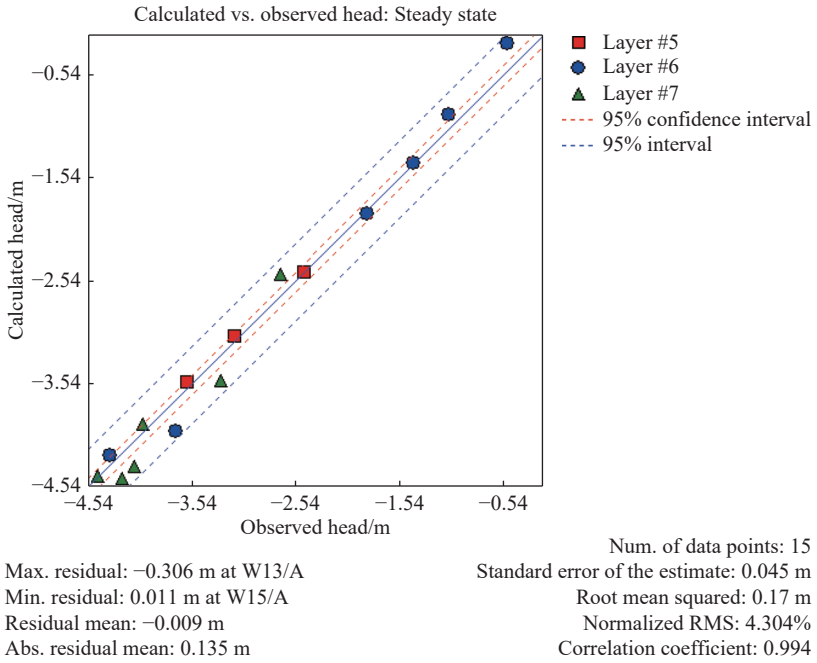


**Fig. 10** Calculated head versus observed head (Sirhan and Koch, 2013) for GCA

−0.306 m to 0.011 m, with a Root Mean Square (RMS) error of 0.17 m and a normalization RMS of 4.304%. These findings indicate a strong correlation ($R^2$ = 0.994) between the model outputs and the measurements from the observation wells, as shown in Fig. 10.

The extent of saltwater intrusion in the Gaza Coastal Aquifer (GCA) was measured based on equi-concentration lines. These measurements revealed intrusion lengths of 3,165 m for the 32,400 ppm (90% saltwater concentration), 4,760 m for the 18,000 ppm (50% saltwater concentration), and 5,450 m for the 3,600 ppm contour (10% saltwater concentration), as shown in Fig. 11.

Fig. 12 displays the input parameters for calculating the saline water intrusion wedge toe for the Gaza coastal aquifer using the constant flux boundary solution of Ataie-Ashtiani et al. (2013) through the web-based interface tool. For constant flux boundary saltwater intrusion problems, the freshwater flux boundary condition is a known input. The parameters include the aquifer length (L = 1,000 m), the aquifer depth from the Mediterranean Sea level to the bottom of the aquifer bed ($Z_o$ = 100 m), the density of freshwater ($\rho_f$ =1.0 gm/cm$^3$), the density of saltwater ($\rho_s$ = 1.025 gm/cm$^3$), the freshwater flux boundary (Q = 1.7 m$^2$/d/m), the hydraulic conductivity of the aquifer medium (K = 0.15 m/d), and the rate of recharge.

Fig. 13 shows the input parameters for calculating the saltwater intrusion wedge toe in the Gaza coastal aquifer using the constant head boundary solution of Ataie-Ashtiani et al. (2013) through the web-based interface tool. For constant head boundary seawater intrusion problems, the flux boundary condition is unknown, but the freshwater head above the mean sea level is known. Firstly, the flux boundary condition is calculated through the built web interface based on the input hydrological parameters, and then the toe location is deter-

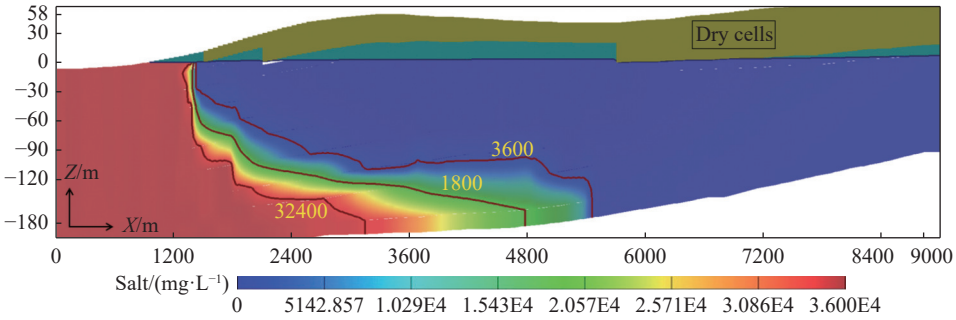


**Fig. 11** Simulated SI in Gaza aquifer for the base case. The contours represent the following concentration levels: 32,400 ppm for the 90% equi-concentration line, 18,000 ppm for the 50% equi-concentration line, and 3,600 ppm for the 10% equi-concentration line

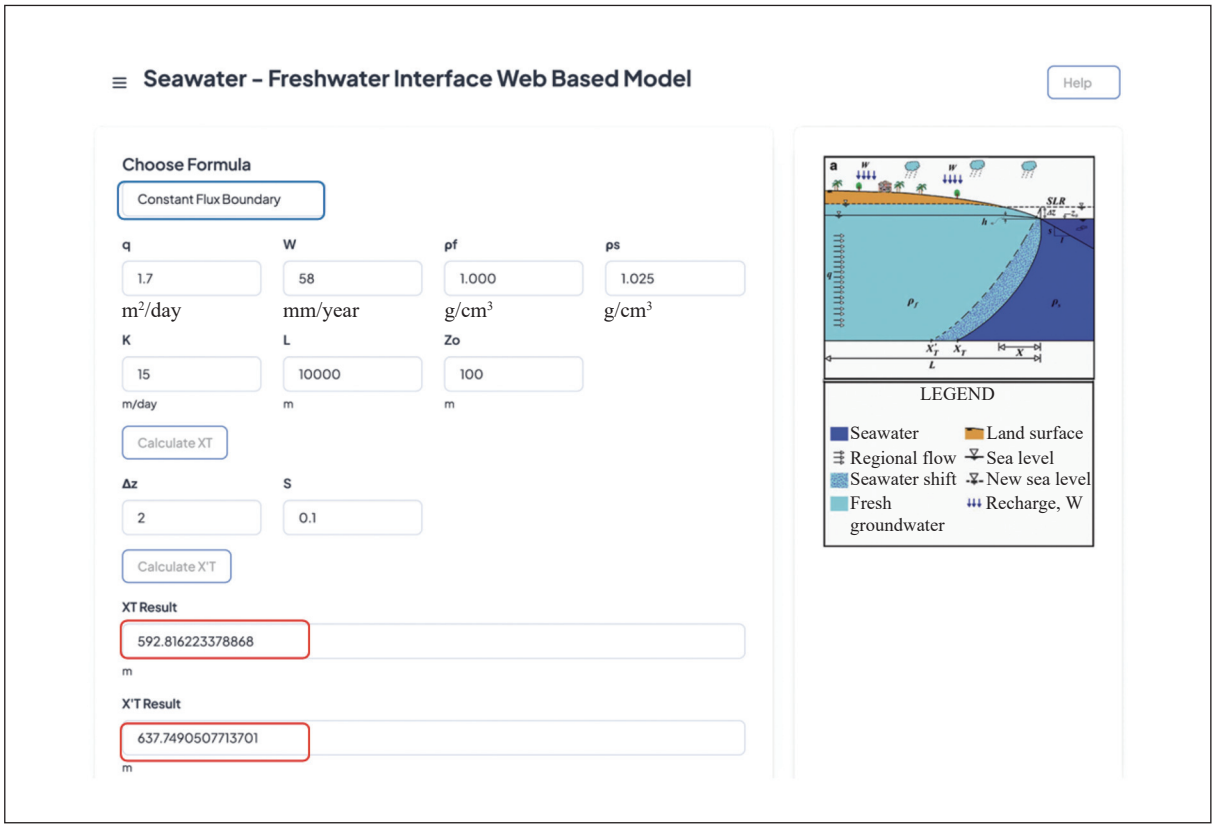


**Fig. 12** Input Parameters for calculating seawater intrusion wedge toe for the Gaza coastal aquifer using Ataie-Ashtiani et al. (2013) through the web-based interface tool for a constant flux boundary problem

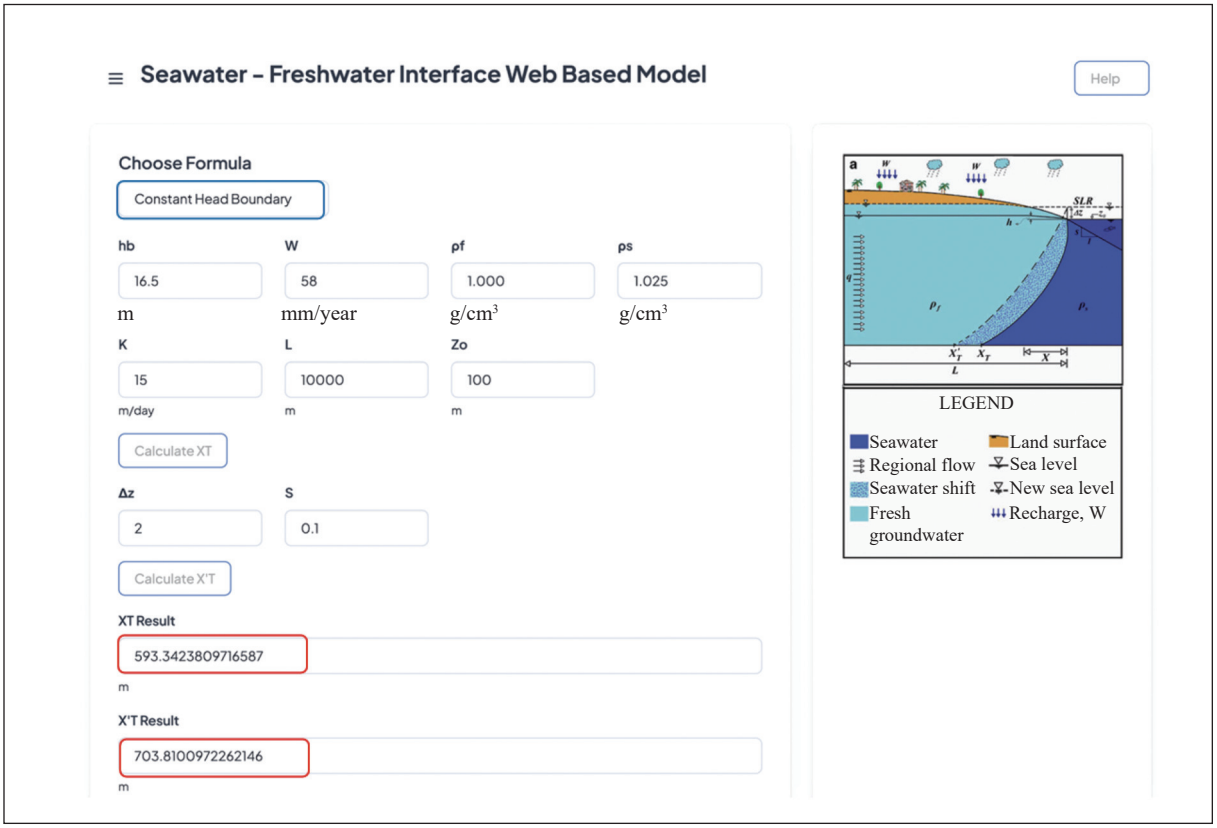


**Fig. 13** Input parameters for calculating seawater intrusion wedge toe for the Gaza coastal aquifer using Ataie-Ashtiani et al. (2013) through the web-based interface tool for a constant head boundary problem

mined. The input parameters include the aquifer length (L = 1,000 m), the depth of the coastal aquifer from the sea level to the groundwater aquifer bottom ($Z_o$ = 100 m), the densities of freshwater ($\rho_f$ =1.0 gm/cm$^3$) and saltwater ($\rho_s$ = 1.025 gm/cm$^3$), the freshwater head overhead mean sea level ($h_f$ = 16 m), the hydraulic conductivity of the aquifer (K = 0.15 m/d), and the rate of recharge. At $Z_o$ = 100 m, the calculated intrusion wedge toe measured from the sea boundary equals 592.8 m and 593.3 m for the constant flux boundary and constant head boundary, respectively.

The web-based interface also calculated the new location of the seawater intrusion wedge toe under various Sea Level Rise (SLR) scenarios (ΔZ). Table 5 presents the input parameters for the Gaza coastal aquifer and the resulting seawater-freshwater toe position (for $Z_o$ = 100 m) compared with the

**Table 5** Parameters for the Gaza Coastal Aquifer and comparison of SW-FW web-based toe position (for Zo = 100 m) with Ataie-Ashtiani et al. (2013)

| No. | K (m/d) | W (mm/a) | $Z_o$ (m) | L (m) | ΔZ | S | Flux BC | | | Head BC | | |
|---|---|---|---|---|---|---|---|---|---|---|---|---|
| | | | | | | | Q (m$^2$/d) | $X_T$ Ataie-Ashtiani et al. (2013) | $X_T$ Current study | $h_b$ (m) | $X_T$ Ataie-Ashtiani et al. (2013) | $X_T$ Current study |
| 1 | 15 | 58 | 100 | 10,000 | 0 | - | 1. 7 | 593 | 592.8 | 16.5 | 593 | 593.34 |
| | | | | | 2 | 0.1 | | 638 | 637.75 | | 704 | 703.81 |
| | | | | | 2 | 0.01 | | 823 | 823.34 | | 878 | 877.71 |
| 2 | 15 | 31 | 100 | 10,000 | 0 | - | 3.4 | 454 | 454.34 | 23.9 | 454 | 454.20 |
| | | | | | 2 | 0.1 | | 493 | 492.97 | | 529 | 529.49 |
| | | | | | 2 | 0.01 | | 675 | 674.70 | | 702 | 702.15 |
| 3 | 15 | 31 | 100 | 10,000 | 0 | - | 1.8 | 734 | 734.06 | 15 | 734 | 732.19 |
| | | | | | 2 | 0.1 | | 785 | 784.59 | | 885 | 884.99 |
| | | | | | 2 | 0.01 | | 969 | 969.14 | | 1055 | 1054.59 |

analytical solutions of Ataie-Ashtiani et al. (2013) for different SLR scenarios. The additional input data required to assess the influence of SLR on the seawater intrusion wedge toe location are the mean seal level rise (ΔZ) and the slope of the sea boundary aquifer bed (s).

Table 5 shows the comparison between the intrusion length for the Gaza coastal aquifer calculated by Ataie-Ashtiani et al. (2013) and the values obtained through the web-based interface tool. The results showed good agreement for a sea level rise of 2.0 m and different values of the sea slope boundary. This agreement is evident for both the constant flux and constant head boundary conditions.

As presented in Table 5, three scenarios for the Gaza coastal aquifers were implemented with varying hydraulic conductivity, groundwater recharge rate, and depth of the aquifer. The groundwater recharge rates were adjusted to 58, 31, and 31 mm/year across the three scenarios, while the aquifer depth and the hydraulic conductivity remained constant. Three sea slopes were considered: 0.0, 0.1, and 0.01, resulting in a total of nine tested scenarios. These adjusted scenarios estimated the intrusion length in the Gaza coastal aquifer for both constant head and constant flux boundary problems.

For scenario No.1, with a constant flux of 1.7 $m^2$/d, the web-based tool calculated seawater intrusion toe lengths of 592.8 m, 637.75 m, and 823.34 m for the bed slopes of 0.0, 0.1, and 0.01, respectively. This compares with 593.34, 703.81, 877.71 m for a head boundary of 16.5 m under the same respective bed slopes. For scenario No.2, with a constant flux of 3.4 $m^2$/day, the web-based tool calculated seawater intrusion toe lengths of 454.34 m, 492.97 m, and 674.7 m for bed slopes of 0.0, 0.1, and 0.01, respectively. This compares with 454.49 m, 529.49 m, and 702.15 m for a constant head boundary of 23.9 m under the same respective bed slopes. For scenario No.3, with a constant flux of 1.8 $m^2$/day, the web-based tool calculated seawater intrusion toe lengths of 734.06 m, 784.59 m, and 969.14 m for the bed slopes of 0.0, 0.1, and 0.01, respectively. This compares with 732.19 m, 887.99 m, and 1054.59 m for a constant head boundary of 15 m under the same respective bed slopes.

Table 6 presents the input parameters for the Gaza coastal aquifer and a comparison of the seawater-freshwater web-based toe position with SEAWAT results (for the 90% concentration = 32400 mg/L, at $Z_o$ = 180 m) under Various Sea-Level rise (SLR). SLR scenarios of 0.5 m, 1.0 m, 1.5 m, and 2.0 m were evaluated using the web-based interface and compared with simulated intrusion lengths from the SEAWAT code. The comparison between the calculated and simulated seawater wedge toe penetration lengths showed a good agreement across different SLR scenarios.

The web-based tool calculated seawater intrusion toe lengths of 2,101 m, 2,119 m, 2,137 m, 2,155 m, and 2,173 m for SLR scenarios of 0.0 m (steady-state), 0.5 m, 1.0 m, 1.5 m, and 2.0 m, respectively. In contrast, the SEAWAT code simulated seawater intrusion wedge toe lengths of 2,208 m (steady-state), 2,216 m, 2,229 m, 2,243 m, and 2,252 m for the same respective SLR scenarios.

Fig. 14 illustrates the seawater intrusion distribution in the Gaza coastal aquifer under steady state conditions and SLR scenarios of 0.5 m, 1.0 m, 1.5 m, and 2.0 m. As the sea level increases, the seawater advances further inland into the Gaza coastal aquifer. According to the SEAWAT simulations, the saltwater intrudes an additional 8 m, 21 m, 35 m, and 44 m for SLR of 0.5 m, 1.0 m, 1.5 m, and 2.0 m, respectively, compared to the steady-state conditions. Similarly, the web-based tool calculations indicate an inland advancement of 18 m, 36 m, 54 m, and 72 m for the same SLR scenarios, respectively, relative to the calculated value by

**Table 6** Parameters for the Gaza Coastal Aquifer and comparison of SW-FW web-based toe position with SEAWAT results (for 90% concentration = 32,400 mg/L at $Z_o$ = 180 m) under various SLR scenarios

| No. | K (m/d) | W (mm/a) | $Z_o$ (m) | L (m) | ΔZ | S | Flux BC | | |
|---|---|---|---|---|---|---|---|---|---|
| | | | | | | | Q ($m^2$/d) | SEAWAT | $X_T$ Current Study (m) |
| 1 | 15 | 58 | 180 | 9,000 | 0 | - | 1.7 | 2,208 | 2,101 |
| | | | | | 0.5 | 0.1 | | 2,216 | 2,119 |
| | | | | | 1.0 | 0.1 | | 2,229 | 2,137 |
| | | | | | 1.5 | 0.1 | | 2,243 | 2,155 |
| | | | | | 2.0 | 0.1 | | 2,252 | 2,173 |

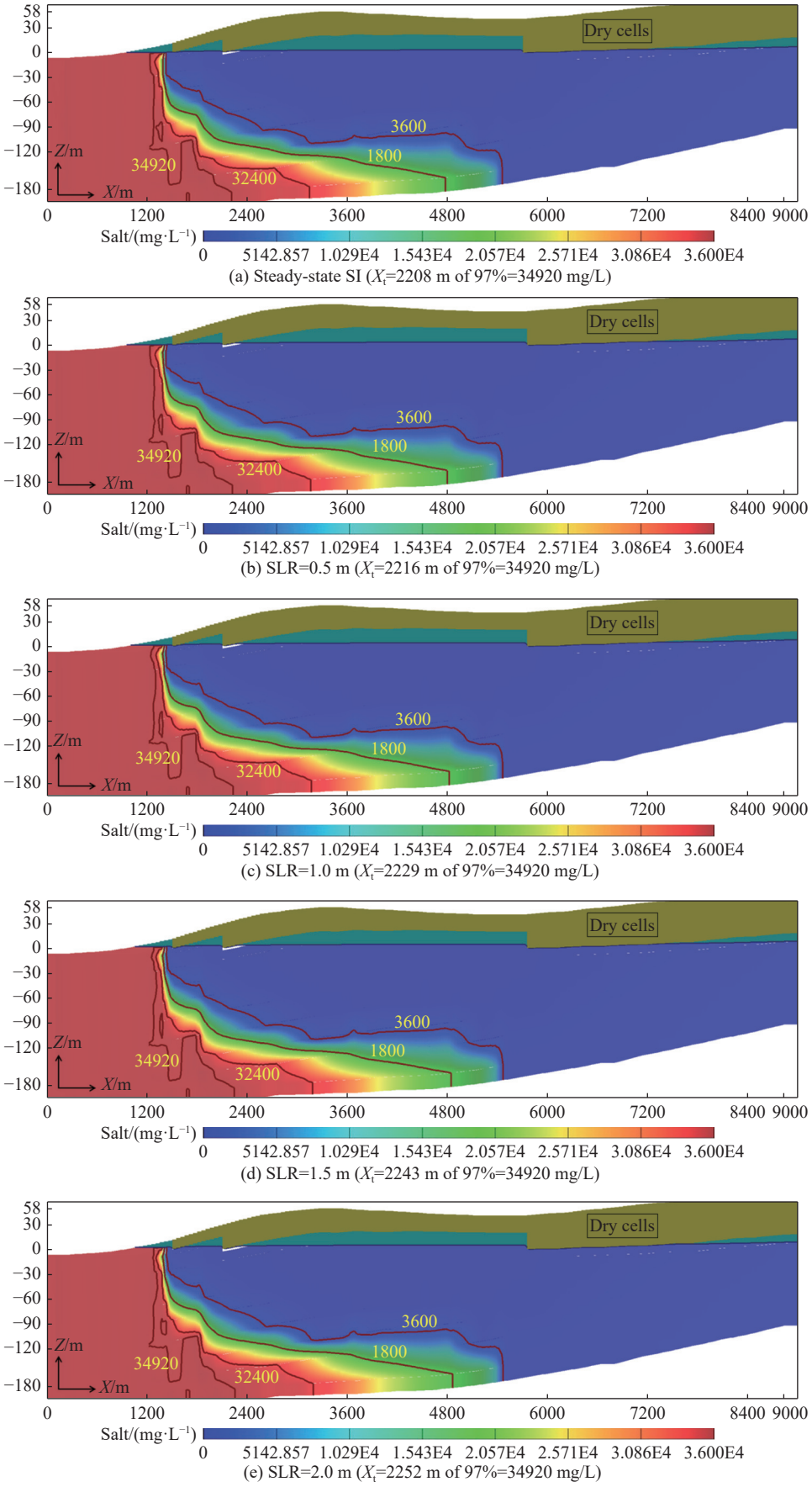


**Fig. 14** Seawater intrusion distribution in the Gaza coastal aquifer: (a) steady-state condition, (b) SLR = 0.5 m, (c) SLR = 1.0 m, (d) SLR = 1.5 m, and (e) SLR = 2.0 m

Ataie-Ashtiani et al. (2013) through the web-based interface tool.

The difference between the simulated intrusion length (SEAWAT) in Gaza coastal aquifers and the estimated value from the analytical solution through the web-based tool is 7.0 m, 97 m, 92 m, 88 m, and 79 m for seal level rise scenarios equals 0.0 m, 0.5 m, 1.0 m, 1.5 m, and 2.0 m, consequentially.

## 4 Conclusion

This study successfully developed and applied a web-based interface tool to illustrate the dynamics of the seawater-freshwater interface using several established analytical solutions. The analytical solutions for constant flux and constant head boundary conditions were compared with the simulated intrusion length of the seawater intrusion wedge obtained from the SEAWAT code. The results generated by the web-based tool, developed in JavaScript, were presented for three distinct case studies: A hypothetical unconfined coastal aquifer, an experimental coastal aquifer, and the Gaza coastal aquifer. Comparison of the analytical solutions with experimental and numerical results for the hypothetical and experimental aquifers revealed that the solutions by Glover and Rumer Jr. and Harleman demonstrated the best agreement. For the Gaza coastal aquifer, the seawater intrusion length calculated using Ataie-Ashtiani's solution showed a strong correlation with the results obtained from the web-based tool, particularly under a 2.0-meter sea-level rise and across a range of sea slope boundary values for both constant flux and constant head boundary conditions. The study confirmed that a rising sea level in the Mediterranean Sea leads to a landward advance of the seawater intrusion wedge toe in the Gaza coastal aquifer. Both the web-based tool predictions and the SEAWAT simulations showed a consistent increase in the seawater intrusion toe length with increasing sea-level rise scenarios. While both approaches exhibited the same trend, SEAWAT simulations generally predicted slightly longer toe lengths compared to the web-based tool. This study provides valuable insights into saltwater intrusion in coastal aquifers. The findings can inform the development of improved management strategies and regulations aimed at addressing and mitigating the adverse effects of this incursion. Additionally, the study effectively examined the impact of sea-level rise on the location of the seawater intrusion toe in the coastal groundwater aquifer system through an accessible web-based interface.

To further enhance the applicability and robustness of the developed tool, future research should focus on several key areas. Incorporating transient conditions into both analytical and numerical models will enable the simulation of more realistic, time-dependent variations in the seawater–freshwater interface. Additionally, conducting thorough sensitivity and uncertainty analyses will provide a deeper understanding of the influence of critical hydrogeological parameters, such as hydraulic conductivity and porosity, on model predictions. Finally, planned improvements to the web-based interface include enhanced interactivity, greater parameter customization, and the dynamic visualization of simulation results.

Web-Based Seawater-Freshwater Interface Link: https://mselmy.github.io/Seawater-Freshwater-Interface-Web-Based-Model/index.html.

## Acknowledgments

This paper is part of a project titled "Optimal Exploitation Strategies for Sustainable Utilization of Fossil Groundwater Reserves in Egypt". It was funded by the Science and Technology Development Fund (STDF)- Egypt (Grant number#46278).

## References

Abd-Elaty I, Zelenakova M. 2022. Saltwater intrusion management in shallow and deep coastal aquifers for high aridity regions. Journal of Hydrology: Regional Studies, 40: 101026. DOI：10.1016/j.ejrh.2022.101026.

Abdoulhalik A, Ahmed AA. 2017. The effectiveness of cutoff walls to control saltwater intrusion in multi-layered coastal aquifers: Experimental and numerical study. Journal of Environmental Management, 199: 62−73. DOI：10.1016/j.jenvman.2017.05.040.

Abualtayef M, Rahman GA, Snounu I, et al. 2017. Evaluation of the effect of water management interventions on water level of Gaza coastal aquifer. Arabian Journal of Geosciences, 10: 1−19. DOI：10.1007/s12517-017-3329-x.

Anderson EI. 2021. Analytical solutions for confined and unconfined coastal interface flow by the Hodograph method. Water Resources Research, 57(9). DOI：10.1029/2021WR030323.

Armanuos AM. 2017. Experimental and numerical study of saltwater intrusion in the Nile delta aquifer, Egypt [PhD Thesis]. Egypt-Japan University of Science and Technology (E-JUST).

Armanuos AM, Al-Ansari N, Yaseen ZM. 2020a. Assessing the effectiveness of using recharge wells for controlling the saltwater intrusion in unconfined coastal aquifers with sloping beds: Numerical Study. Sustainability, 12(7): 2685. DOI：10.3390/su12072685.

Armanuos AM, Al-Ansari N, Yaseen ZM. 2020b. Underground barrier wall evaluation for controlling saltwater intrusion in sloping unconfined coastal aquifers. Water, 12(9): 2403. DOI：10.3390/w12092403.

Ataie-Ashtiani B, Werner AD, Simmons CT, et al. 2013. How important is the impact of land-surface inundation on seawater intrusion caused by sea-level rise? Hydrogeology Journal, 21(7): 1673.

Chang SW, Clement TP, Simpson MJ, et al. 2011. Does sea-level rise have an impact on saltwater intrusion? Advances in Water Resources, 34(10): 1283–1291. DOI：10.1016/j.advwatres.2011.06.006.

Dang NM, Vien LN, Tung NB, et al. 2020. Assessments of climate change and sea level rise impacts on flows and saltwater intrusion in the Vu Gia—Thu Bon River Basin, Vietnam. APAC. Springer Singapore: 1367–1374. DOI: 10.1007/978-981-15-0291-0_185

Emara SR, Armanuos AM, Gado TA, et al. 2023a. Verification of experimental saltwater intrusion interface in unconfined coastal aquifers using numerical and analytical solutions. Acque Sotterranee - Italian Journal of Groundwater, 12(3): 23−38. DOI：10.7343/as-2023-668.

Emara SR, Armanuos AM, Shalby A. 2024a. Appraisal seawater intrusion vulnerability for the Moghra coastal aquifer, Egypt– application of the GALDIT index, sensitivity analysis, and hydro-chemical indicators. Groundwater for Sustainable Development, 25: 101166. DOI：10.1016/j.gsd.2024.101166.

Emara SR, Armanuos AM, Zeidan BA, et al. 2024b. Numerical investigation of mixed physical barriers for saltwater removal in coastal heterogeneous aquifers. Environmental Science and Pollution Research, 31(3): 4826−4847. DOI：10.1007/s11356-023-31454-z.

Emara SR, Gado TA, Zeidan BA, et al. 2023b. Evaluating the impact of inclined cutoff-wall to control seawater intrusion in heterogeneous coastal aquifers. Water Resources Management, 37(15): 6021−6050. DOI：10.1007/s11269-023-03641-7.

Fan Y, Lu W, Miao T, et al. 2020. Multiobjective optimization of the groundwater exploitation layout in coastal areas based on multiple surrogate models. Environmental Science and Pollution Research, 27(16): 19561−19576. DOI：10.1007/s11356-020-08367-2.

Ghyben BW. 1888. Nota in verband met de voorgenomen putboring nabij, Amsterdam. The Hague, 21.

Glover RE. 1959. The pattern of fresh-water flow in a coastal aquifer. Journal of Geophysical Research, 64(4): 457−459. DOI：10.1029/JZ064i004p00457.

Goswami RR, Clement TP. 2007. Laboratory-scale investigation of saltwater intrusion dynamics. Water Resources Research, 43. DOI：10.1029/2006WR005151.

Guo W, Langevin CD. 2002. User's guide to SEAWAT; a computer program for simulation of three-dimensional variable-density ground-water flow (USGS Numbered Series No. 06-A7), User's guide to SEAWAT; a computer program for simulation of three-dimensional variable-density ground-water flow, Techniques of Water-Resources Investigations. DOI：10.3133/twri06A7.

Heen ZHA, Muhsen S. 2016. Application of vertical electrical sounding for delineation of sea water intrusion into the freshwater aquifer of southern governorates of Gaza Strip, Palestine. IUG Journal of Natural Studies, 24(2).

Herzberg A. 1901. Die wasserversorgung einiger Nordseebader. Journal für Gasbeleuchtung und Wasserversorgung, 44: 842−844.

Javadi A, Hussain M, Sherif M, et al. 2015. Multi-objective optimization of different management scenarios to control seawater intrusion in coastal aquifers. Water Resources Management, 29(6): 1843−1857. DOI：10.1007/s11269-015-0914-1.

Kaleris VK, Ziogas AI. 2013. The effect of cutoff

walls on saltwater intrusion and groundwater extraction in coastal aquifers. Journal of Hydrology, 476: 370−383. DOI：10.1016/j.jhydrol.2012.11.007.

Koussis AD, Mazi K, Destouni G. 2012. Analytical single-potential, sharp-interface solutions for regional seawater intrusion in sloping unconfined coastal aquifers, with pumping and recharge. Journal of Hydrology, 416–417: 1–11. DOI：10.1016/j.jhydrol.2011.11.012.

Kuan WK, Jin G, Xin P, et al. 2012. Tidal influence on seawater intrusion in unconfined coastal aquifers. Water Resources Research, 48(2): 136−149. DOI：10.1029/2011WR010678.

Li Y, Wen MZ, Yu H, et al. 2024. Changes of coastline and tidal flat and its implication for ecological protection under human activities: Take China's Bohai Bay as an example. China Geology, 7(1): 26−35. DOI：10.31035/cg2023007.

Lu C, Xin P, Li L, et al. 2015. Seawater intrusion in response to sea-level rise in a coastal aquifer with a general-head inland boundary. Journal of Hydrology, 522: 135−140.

Lu C, Xin P, Kong J, et al. 2016. Analytical solutions of seawater intrusion in sloping confined and unconfined coastal aquifers. Water Resources Research, 52(9): 6989−7004. DOI：10.1002/2016WR019101.

Luo Z, Kong J, Shen C, et al. 2022. Approximate analytical solutions for assessing the effects of unsaturated flow on seawater extent in thin unconfined coastal aquifers. Advances in Water Resources, 160: 104104. DOI：10.1016/j.advwatres.2021.104104.

Mehdizadeh SS, Badaruddin S, Khatibi S. 2019. Abstraction, desalination and recharge method to control seawater intrusion into unconfined coastal aquifers. Global Journal of Environmental Science and Management, 5(1): 107−118. DOI：10.22034/gjesm.2019.01.09.

Motallebian M, Ahmadi H, Raoof A, et al. 2019. An alternative approach to control saltwater intrusion in coastal aquifers using a freshwater surface recharge canal. Journal of Contaminant Hydrology, 222: 56−64. DOI：10.1016/j.jconhyd.2019.02.007.

Qahman K. 2004. Aspects of hydrogeology, modeling, and management of seawater intrusion for Gaza aquifer–palestine. PhD. theis, LIMEN, Ecole Mohammadia D 'Ingenieurs, Université Mohammed V-Morocco.

Ranjbar A, Mahjouri N, Cherubini C. 2020. Development of an efficient conjunctive meta-model-based decision-making framework for saltwater intrusion management in coastal aquifers. Journal of Hydro-Environment Research, 29: 45−58. DOI：10.1016/j.jher.2019.11.005.

Rumer Jr RR, Harleman DR. 1963. Intruded saltwater wedge in porous media. Journal of the Hydraulics Division, 89(6): 193−220. DOI：10.1061/JYCEAJ.0000954.

Sherif M, Sefelnasr A, Ebraheem AA, et al. 2014. Quantitative and qualitative assessment of seawater intrusion in Wadi Ham under different pumping scenarios. Journal of Hydrologic Engineering, 19(5): 855−866. DOI：10.1061/(ASCE)HE.1943-5584.0000907.

Sirhan H, Koch M. 2013. Numerical modeling of the effects of artificial recharge on hydraulic heads in constant-density ground water flow to manage the Gaza coastal aquifer, South Palestine. 6th International Conference on Water Resources and Environment Research, ICWRER: 3−7.

Sun Q, Zheng T, Zheng X, et al. 2021. Effects of subsurface barriers on seawater intrusion and nitrate accumulation in coastal aquifers. Authorea Preprints. DOI：10.22541/au.161252403.31172601.

Verruijt A. 1968. A note on the Ghyben-Herzberg formula. Hydrological Sciences Journal, 13(4): 43−46.

Wang XJ, Guo YF, Yu SC, et al. 2025. Nutrient dynamics and discharge in a coastal sandy beach aquifer. Hydrogeology & Engineering Geology, 52(1): 12−22. DOI：10.16030/j.cnki.issn.1000-3665.202409063.

Werner AD, Bakker M, Post VEA, et al. 2013. Seawater intrusion processes, investigation and management: Recent advances and future challenges. Advances in Water Resources, 51: 3−26. DOI：10.1016/j.advwatres.2012.03.004.